



HAL
open science

Finite Element Simulation of Laser Beam Welding Induced Residual Stresses and Distortions in a T-Joint Configuration for Aeronautic Structures

Muhammad Zain-Ul-Abdein, Daniel Nélias, Jean-François Jullien, Dominique Deloison

► **To cite this version:**

Muhammad Zain-Ul-Abdein, Daniel Nélias, Jean-François Jullien, Dominique Deloison. Finite Element Simulation of Laser Beam Welding Induced Residual Stresses and Distortions in a T-Joint Configuration for Aeronautic Structures. ASME 2009 Pressure Vessels and Piping Conference, Jul 2009, Prague, Czech Republic. pp.371-379, 10.1115/PVP2009-77310 . hal-04711633

HAL Id: hal-04711633

<https://hal.science/hal-04711633v1>

Submitted on 2 Jan 2025

HAL is a multi-disciplinary open access archive for the deposit and dissemination of scientific research documents, whether they are published or not. The documents may come from teaching and research institutions in France or abroad, or from public or private research centers.

L'archive ouverte pluridisciplinaire **HAL**, est destinée au dépôt et à la diffusion de documents scientifiques de niveau recherche, publiés ou non, émanant des établissements d'enseignement et de recherche français ou étrangers, des laboratoires publics ou privés.



Distributed under a Creative Commons Attribution - NonCommercial 4.0 International License

FINITE ELEMENT SIMULATION OF LASER BEAM WELDING INDUCED RESIDUAL STRESSES AND DISTORTIONS IN A T-JOINT CONFIGURATION FOR AERONAUTIC STRUCTURES**Muhammad Zain-ul-abdein**LaMCoS, INSA-Lyon
CNRS UMR5259
F69621, France**Daniel Nélias**LaMCoS, INSA-Lyon
CNRS UMR5259
F69621, France**Jean-François Jullien**LaMCoS, INSA-Lyon
CNRS UMR5259
F69621, France**Dominique Deloison**EADS Innovation Works
12 Rue Pasteur, BP76,
92152 Suresnes Cedex, France**ABSTRACT**

Laser beam welding has found its application in the aircraft industry for the fabrication of fuselage panels in a T-joint configuration. However, the inconveniences like distortions and residual stresses are inevitable consequences of welding. The effort is made in this work to experimentally measure and numerically simulate the distortions induced by laser beam welding of a T-joint with industrially used thermal and mechanical boundary conditions on the thin sheets of aluminium 6056-T4. Several small scale experiments were carried out with various instrumentations to establish a database necessary to verify the simulation results. Finite element (FE) simulation is performed with Abaqus and the conical heat source is programmed in FORTRAN. Heat transfer analysis is performed to achieve the required weld pool geometry and temperature fields. Mechanical analysis is then performed with industrial loading and boundary conditions so as to predict the distortion and the residual stress pattern. A good agreement is found amongst the experimental and simulation results.

Keywords: laser beam welding, thermo-mechanical analysis, residual stress, distortion

INTRODUCTION

The aerospace industry is constantly coping with the challenges like reduction in weight of an aircraft structure. The fabrication of fuselage panels has so far been carried out through riveting; a process that essentially adds up a huge amount of unwanted material, thereby, considerably increasing the overall weight of the structure. The new generation aircraft structures are, therefore, now being manufactured by laser-beam welding so as to get rid off the additional material added in the form of rivets. Moreover, the production rate is improved due to high speed welding process. The fuselage panels are large thin structures of Al 6056T4 (an aluminium alloy) with stiffeners welded upon them. The typical length of weld seam reaches 50 m or so. Industrially, the fuselage panels are held in position with the help of a suction table. Laser-beam welding is employed in a key-hole regime. The stiffeners are welded with fuselage panels using two laser beams moving simultaneously on each side of the T-joint; the test case presented here replicates the identical situation. Such a configuration helps creating even pull on each side thereby minimising distortions. However, by the very nature of the process, welding induces highly non-uniform residual stresses and distortions in the structure. In

the recent years, numerical simulation has proven itself to be a useful tool in predicting these welding-induced distortions and residual stresses. The knowledge of residual stress distribution and distortions may then lead to the better control over the undesirable aspects of the process.

Numerical simulation of laser beam welding involves several complex phenomena like formation of a key-hole, ionization and vaporization of material, circulation of molten material within the weld pool due to electromagnetic and buoyancy forces (Marangoni effect), solidification at the liquid-solid interface etc. Sudnik et al. [1] discussed the mathematical model of key-hole formation and studied the simulation of weld pool geometry with key-hole formation and varying welding parameters namely laser beam power and welding speed. According to their findings, there exists a linear relationship between the length and depth of the weld pool for laser beam welding experiments with varied laser beam power and constant welding speed; while on the other hand, the weld pool length changes slightly with varying welding speed and constant laser beam power. Jin et al. [2] focussed upon heat transfer model based on an actual key-hole and discussed the thermal gradient and melt pool shape around the key-hole on the surface of the test specimen. Olmedo [3] also discussed the principal of laser beam welding with special reference to aluminium alloys used for aeronautical applications. Comparison between experimental and simulated results for distortions is developed by Tsirkas et al. [4] who used the commercial software SYSWELD for simulation. Darcourt et al. [5] attempted to predict laser beam welding induced distortions for a T-joint and suggested that a correct thermal analysis is mandatory to predict welding induced distortions and residual stresses. Jossierand et al. [6] have also tried to predict laser welding induced-distortions for an aeronautic aluminium alloy while working on thin test plates. They have suggested that the initial surface profiles of the test plate due to pre-processing, like rolling etc., play an important role in defining the distortions level of test plate. Zaeem et al. [7] have also tried to predict welding buckling distortion in thin walled aluminium T-joint. The integration of thermo-metallo-mechanical behaviour of material makes the simulation techniques more complicated. Moreover, numerical simulation of large structures

with three dimensional continuum elements entails the use of exceptionally powerful computers, yet the computation time may prolong up to several days or weeks. Efforts are, therefore, made to introduce several simplifications during simulation so as to deal with the problem of excessive computation time without compromising the quality of results.

The work presented here is a part of the project INZAT4, sponsored by EADS, AREVA-NP, EDF, ESI Group and Rhône-Alpes Région and encompasses the finite element simulation of laser-beam welded T-joints of thin sheets of Al 6056T4. An instrumented experimental campaign was first carried out in order to establish the database necessary for the validation of simulation results. A part of this work has also been presented in [8] where fusion pass welding of test plates was studied.

EXPERIMENTAL CAMPAIGN

The laser-beam welding of T-joints is performed over small scale specimens. Efforts are made to integrate the industrially used thermal and mechanical boundary conditions. The test case presented here includes welding of a base plate of dimensions 300 mm x 200 mm x 2.5 mm with a stiffener of dimensions 300 mm x 100 mm x 2.5 mm in a T-joint assembly.

Laser-beam welding was performed simultaneously on both sides of T-joint with the addition of filler metal wire. Various instruments were used before, during and after the welding in order to capture maximum information in terms of temperatures and displacement fields. Thermocouples (TCs) were installed to record the temperatures on the upper and lower surfaces of the base plate and on the stiffener. Infra-red camera was also installed to observe the evolution of surface temperature of weld pool during welding. The speckle pattern was created on both sides of weld fusion line to perform 3D image-correlation in order to get the displacement fields of the upper surface of the base plate before and after welding. Macrographs were finally taken to measure the dimensions of weld pool. The base plate was mounted on an aluminium suction table by means of suction force (≈ 1 bar) applied through the grooves provided in the table on the bottom side of

the base plate. While the stiffener was placed vertically with the help of fixtures in the middle of the base plate and two concentrated forces each of 50 N were applied on the top of it so as to avoid its separation from the base plate during welding. The geometry of the T-joint assembly and instrumentations are shown schematically in Fig. 1. The experimental setup is also shown.

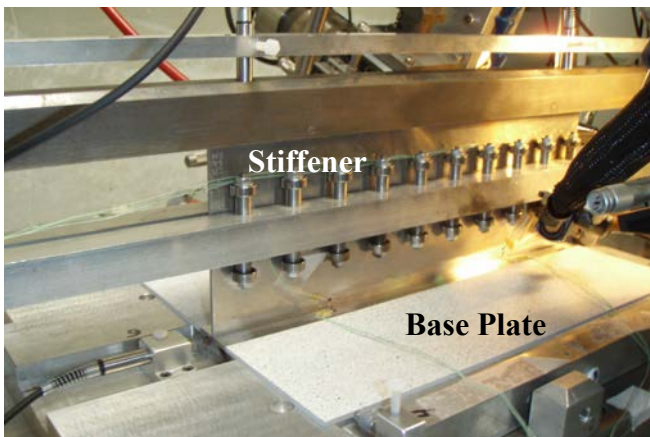
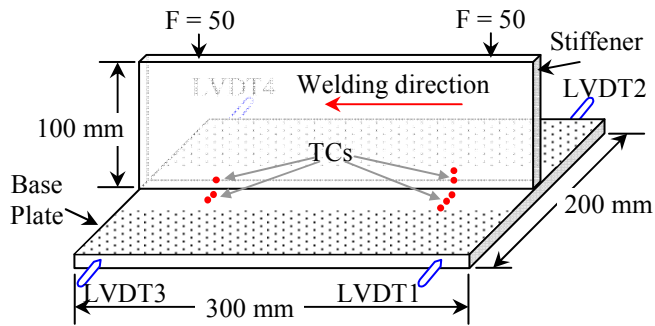


Fig. 1. Schematic representation of T-joint assembly (above), Experimental setup (below)

The bold spots marked as TCs and pointers marked as LVDTs are indicative of thermocouple and LVDT sensor positions respectively; while black dots represent speckle pattern required to perform stereo image correlation. A total of eleven thermocouples were installed on the base plate and stiffener in the vicinity of weld joint. Thermocouples named as TC1, TC2, TC3, TC4 and TC5 were installed on the upper surface of base plate, while TC7 and TC8 were installed on the bottom surface and TC6 was installed in a depth of 0.5 mm beneath the weld line. Similarly TC9, TC10 and TC11 were installed on the stiffener. A set of LVDTs 1 and 2 was placed in line on the base plate close to the welding start position to measure the in-plane displacements during welding. Likewise another set of LVDTs 3 and 4 was placed close to

the welding end position. The average of each set is to be compared later with numerical simulation results. Laser-beam welding in key-hole regime was performed using the following parameters:

- Power (of each welding torch), $P = 2500$ W
- Weld speed, $v = 5$ m/min
- Wire feed rate = 3 m/min
- Wire diameter = 1 mm
- Wire material = Al 4047
- Argon gas flow rate = 20 l/min

As the base plate was placed on an aluminium support during welding, it is expected that a considerable amount of heat energy may dissipate due to the contact between the surfaces. Moreover, the friction present at the plate-support interface is also taken into consideration. It was developed in [8] that the suitable value of friction coefficient to be used is $\mu = 0.57$, however it plays a rather little role on the numerical results. The experimental results will be presented in comparison with FE simulation results.

FINITE ELEMENT SIMULATION

Finite element (FE) simulation is performed on Abaqus /Standard. Owing to the symmetry of T-joint in the welding direction, a symmetric model is considered where base plate, stiffener and filler wire are meshed as a one part assembly. Selection of a symmetric model helps in reducing the number of degrees of freedom thereby reducing the overall computation time. The FE mesh consists of 8-nodes linear brick elements and some 6-node linear prism elements totalling over 76,000 nodes and 63,000 elements. A very fine mesh size is used in the fusion zone where the dimensions of smallest element are 0.5 mm x 0.38 mm x 0.24 mm. The mesh density decreases away from the fusion zone. This is done because of the fact that the temperature gradient is quite high in the fusion and heat-affected zones which in turn gives rise to significantly high stress gradient. The mesh size used for the support is comparatively larger and only 8-nodes linear brick elements are used.

The mesh details are shown in Fig. 2. The zoomed part of the fusion zone shows some highlighted elements. These elements represent filler metal wire, and the effect of filler wire

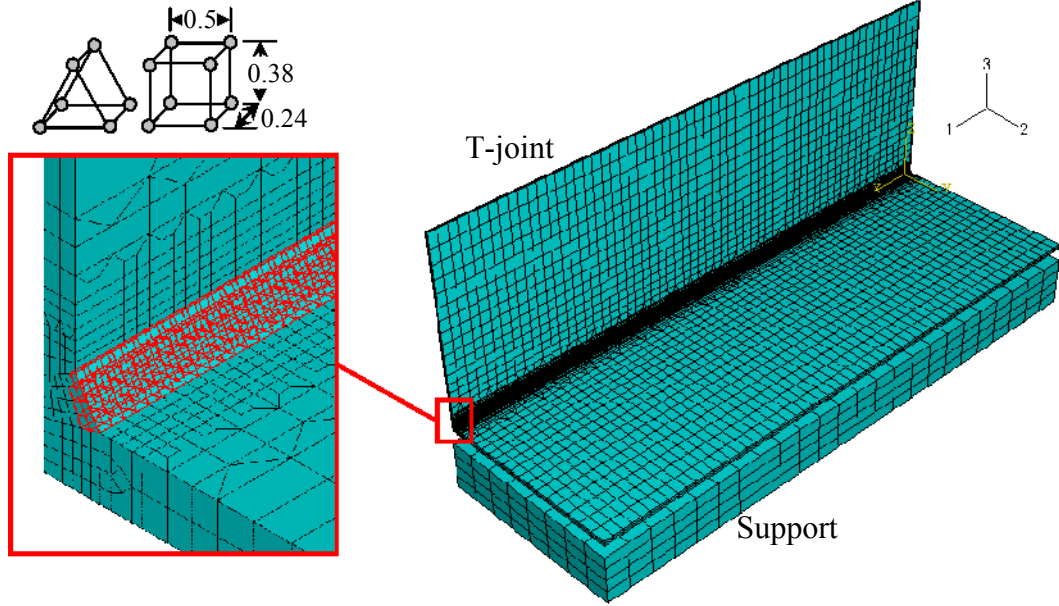


Fig. 2. T-joint and support mesh, zoomed region showing filler wire elements

addition is achieved upon these elements by initial deactivation and temperature dependant activation during welding.

The simulation task is carried out through an uncoupled temperature-displacement analysis, where the thermal analysis is first performed separately in order to adjust the heat source parameters and incorporate the complex thermal boundary conditions including free convection, radiation and thermal contact resistance between the base plate and the support. Temperature histories calculated during thermal analysis are then used as a predefined field for mechanical analysis. Other mechanical boundary conditions and loadings are applied during mechanical analysis.

THERMAL ANALYSIS

The thermal analysis is performed using temperature dependent thermal properties and DC3D8 and DC3D6 type elements with linear interpolation between the nodes. Modelling of a moving heat source is carried out in a FORTRAN based subroutine called DFLUX. Various models ranging from cone-shaped volumetric heat source with Gaussian distribution to double-ellipsoidal volumetric heat source in accordance with Goldak et al. [9] exist to apply the heat flux as accurately as possible. The choice of an appropriate model is

largely dependent upon the weld pool geometry, thermal fields, welding process being simulated etc. In this work a cone-shaped volumetric heat source with Gaussian distribution is used. Owing to the symmetry of T-joint, the heat source applied on one side of the fillet essentially implies the presence of a similar heat source on the other side of the fillet. The heat source model is shown in Fig. 3. Equation (1) presents the heat source formulation.

$$Q_v = \frac{9Q_0}{\pi(1-e^{-3})} \cdot \frac{1}{(z_e - z_i)(r_e^2 + r_e r_i + r_i^2)} \cdot \exp\left(-\frac{3r^2}{r_c^2}\right) \quad (1)$$

where,

$$Q_0 = \eta P$$

and, $r_c = f(z) = r_i + (r_e - r_i) \frac{z - z_i}{z_e - z_i}$

Here, Q_v is the total volumetric heat flux in $W.m^{-3}$, Q_0 is the net heat flux in W, P is the laser beam power in W, η is the efficiency of the process, r is the current radius as a function of Cartesian coordinates x and y , r_c is the flux distribution parameter for the cone as a function of depth (z), r_e and r_i are larger and smaller radii of the cone, respectively. Similarly, z_e and z_i are upper and lower

z -coordinates of the cone, respectively. The parameters are also shown in Fig. 3.

An efficiency (η) of 80 % is used for the thermal analysis with power (P) of 2500 W. The remaining parameters are adjusted to obtain the required weld pool geometry. A latent heat of fusion of $4 \times 10^5 \text{ J.kg}^{-1}$ is used between the solidus and liquidus temperature of $587 \text{ }^\circ\text{C}$ and $644 \text{ }^\circ\text{C}$, respectively.

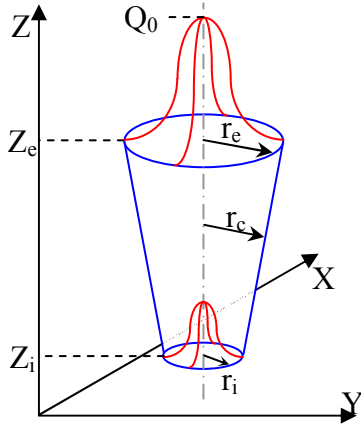


Fig. 3. Heat source model

The thermal boundary conditions are shown in Fig. 4 where cross-sectional view of T-joint is shown. The term $q_{conv+rad}$ present heat transfer due to free convection and radiation in air, the black stripe depicts heat transfer due to thermal conductance at the interface of T-joint and support (q_{cond}) and white stripe shows no heat loss from the plane of symmetry ($q = 0$).

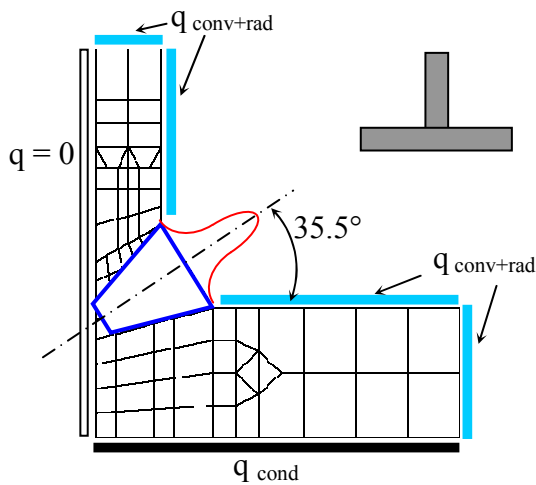


Fig. 4. Schematic sketch showing integration of heat source and thermal boundary conditions and chamfer details on upper right corner (not drawn on scale)

Equations (2) and (3) define $q_{conv+rad}$ and q_{cond} as general boundary conditions.

$$q_{conv+rad} = h_{conv}(T - T_0) + \sigma \varepsilon ((T - T_{abs})^4 - (T_0 - T_{abs})^4) \quad (2)$$

$$q_{cond} = h_{cond}(T_s - T) \quad (3)$$

Here, T , T_0 , T_{abs} and T_s are the temperature of the T-joint, ambient temperature, absolute zero and temperature of the support respectively. The values used for the heat transfer coefficients and radiation constants are as follows:

- Convective heat transfer coefficient of air, $h_{conv} = 15 \text{ W.K}^{-1}.\text{m}^{-2}$
- Emissivity of aluminium surface, $\varepsilon = 0.08$
- Emissivity of speckle pattern, $\varepsilon = 0.71$
- Stefan-Boltzmann constant, $\sigma = 5.68 \times 10^{-8} \text{ J.K}^{-4}.\text{m}^{-2}.\text{s}^{-1}$
- Heat transfer coefficient at the interface of the test plate and support, $h_{cond} = 250 \text{ W.K}^{-1}.\text{m}^{-2}$ at 0 bar, $284 \text{ W.K}^{-1}.\text{m}^{-2}$ at 1 bar

The results of heat transfer analysis are now being presented in comparison with experimental results. The fusion zone observed experimentally from micrographs is placed side by side with simulated weld pool in Fig. 5. The grey coloured region of simulated results shows the shape of fusion zone.

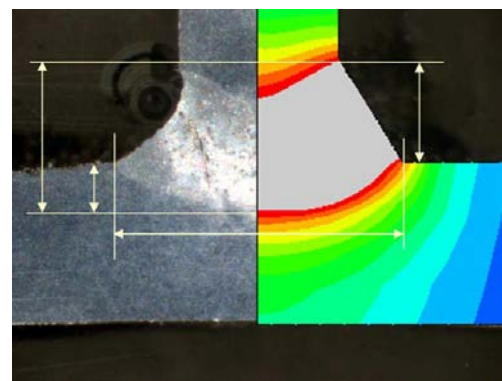


Fig. 5. Experimental vs simulated fusion zone

The temperature histories recorded on thermocouple positions during experimentation are compared with FE simulation results. The comparison at positions TC1, TC2 and TC3 at the upper surface of base plate is shown in Fig. 6.

The comparative analyses for weld pool geometry and thermal histories at specific locations show good accord amongst experimental and simulation results. A few discrepancies observed may be assigned to the simplifications assumed during simulation and minute inaccuracies in positioning of thermocouples. However, the overall simulated temperature fields are good enough to perform mechanical analysis.

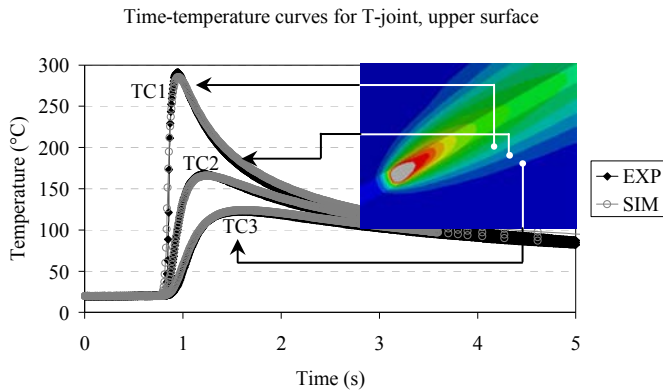


Fig. 6. Temperature histories at TC1, TC2 and TC3 for T-joint upper surface; (Exp vs Sim)

MECHANICAL ANALYSIS

Temperature fields obtained during simulation are used as a predefined field for mechanical analysis. The element types used are C3D8R and C3D6. Following type of mechanical loads and boundary conditions are used.

- Concentrated Force: $F = 50\text{N}$ (applied on both ends of stiffener to avoid its separation from base plate during welding. Fig. 1)
- Uniformly distributed pressure: $p = 0.8\text{ bar}$ (applied on the bottom surface of base plate to include the effect of suction force applied through the aluminium suction table)
- Gravity: $g = 9.8\text{ m.s}^{-2}$
- Coefficient of friction: $\mu = 0.57$ (due to the contact between T-joint and aluminium suction table)
- Symmetric plane condition: $U_y = 0$ (applied on the plane of symmetry along the weld axis for T-joint and support)
- Fixed nodes: $U_x = U_z = 0$ (applied at a node of T-joint near the weld start point; applied at several nodes of support)

The T-joint material is assumed to follow an elasto-plastic law with isotropic hardening behaviour (Mises plasticity model). Certain simplifications are also supposed for simulation such as during experimentation the stiffener was not the part of base plate; however, base plate and stiffener are modelled as a single part for FE simulation. Similarly, the filler wire material (Al 4047) was different from the material of T-joint (Al 6056 T4) for experimental work; yet while performing simulation the former is considered to be the same as the later. The effect of filler wire addition is achieved by initially deactivating some of the elements, which represent wire material, and then by activating them during cooling. From practical point of view, when filler wire becomes part of solidifying weld bead only then it may affect the distortion and stress level of T-joint; this is why the elements representing wire material activate during cooling only and contribute towards the final residual stress state.

The simulation results are now being compared with the experimental results in the following. Figure 7 shows comparison between experimental and simulated results for the displacements recorded by LVDTs during welding. As shown in Fig. 1 the set of LVDT 1 and 2 was placed in line across the base plate opposite to each other, therefore the average of the displacements values measured by each LVDT is compared with simulated values where the FE model is symmetric. Same is the case with another set of LVDTs 3 and 4. It may be observed that the expansion and contraction of base plate during welding and cooling respectively is efficiently captured with FE simulation.

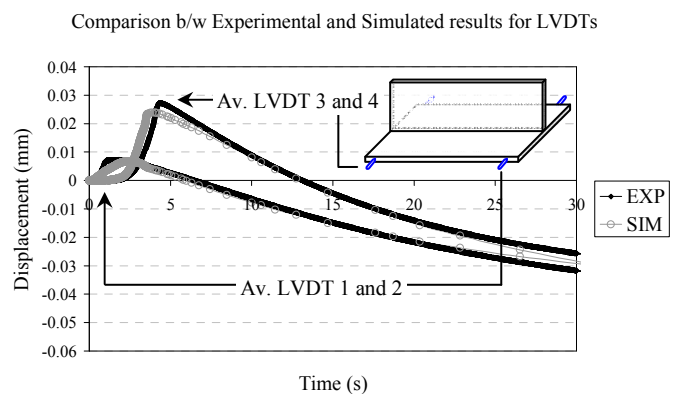


Fig. 7. In-plane displacements during welding at LVDT positions; (Exp vs Sim)

Figure 8 presents the comparison between experimental and simulation results for in-plane displacements measured at the end of welding by image correlation technique. The reference line at which values are compared is also shown in the legend.

It is to be noted that these displacements are actually the ones remaining in the T-joint assembly after removal of all the thermal and mechanical loading and boundary conditions, which implies that these displacements are the permanent distortions induced during welding. An overall good accordance is found amongst experimental and simulation results.

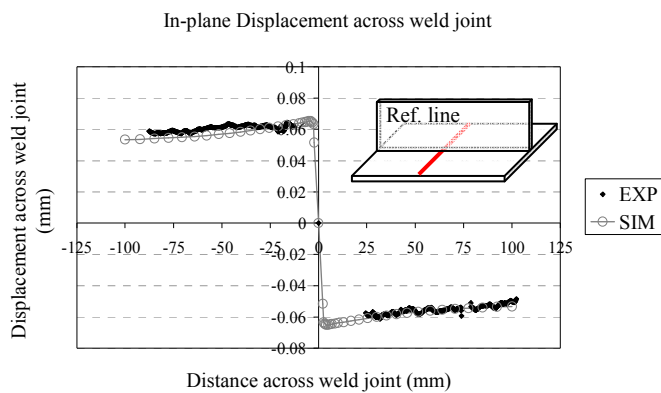


Fig. 8. Residual In-plane displacements; (Exp vs Sim)

Having obtained the good accordance between experimental and simulated temperature and displacement results, residual stresses may now be presented. Figure 9 shows the magnitude of the predicted residual stresses present in the upper surface of the base plate.

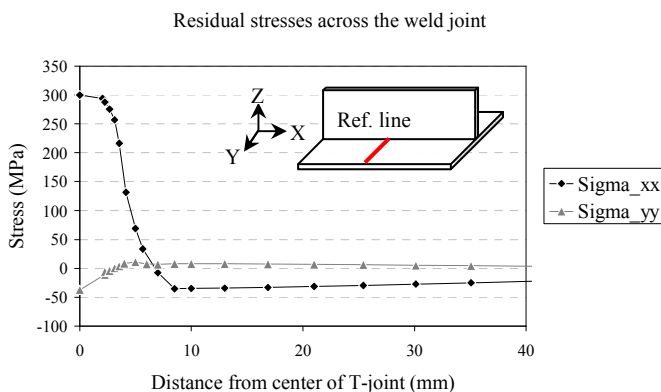


Fig. 9. Longitudinal (σ_{xx}) and Transverse (σ_{yy}) Residual Stresses

These stresses are presented for the symmetric part of the T-joint only. It is found that the longitudinal residual stresses (σ_{xx} , stresses in the direction of welding) have the magnitude approaching 300 MPa in the fusion zone and are largely tensile in nature; however these stresses tend to be compressive in heat affected zone (HAZ). On the other hand, the transverse stresses (σ_{yy} , stresses across the weld joint) are mainly compressive in fusion zone and are almost zero in HAZ. All the remaining components of the stress tensor are negligibly small.

The contours of longitudinal and transverse residual stress profiles presented in Fig. 10 depict a region of consistent stress distribution midway between the welding start and stop ends. These are the regions where stress levels reach their maximum values and, hence, are of significance importance. For instance, the longitudinal stress value in this region is as high as yield stress of material and will, therefore, have considerable influence over the failure of material.

Control of welding-induced distortions is a major concern in the aeronautic industry, especially because laser-beam-welded fuselage panels are rather large and thin, and thus prone to buckling. Success with heat sink welding has been reported; yet the current approach to reduce distortion is based on local post-welding mechanical treatment (shot peening) and optimisation of geometry.

CONCLUSIONS

A comparative study of experimental and numerical simulation results has been carried out. Following conclusions are inferred:

1. Good agreement is found between experimentally observed and simulated weld pool geometry; which justifies the integration of conical heat source model. Likewise, a good accordance is found for thermal histories between experimental and FE simulation results; which, in turn, verifies the accuracy of applied heat flux and thermal boundary conditions including thermal contact resistance. A few discrepancies may be attributed to the simplifications assumed during simulation.

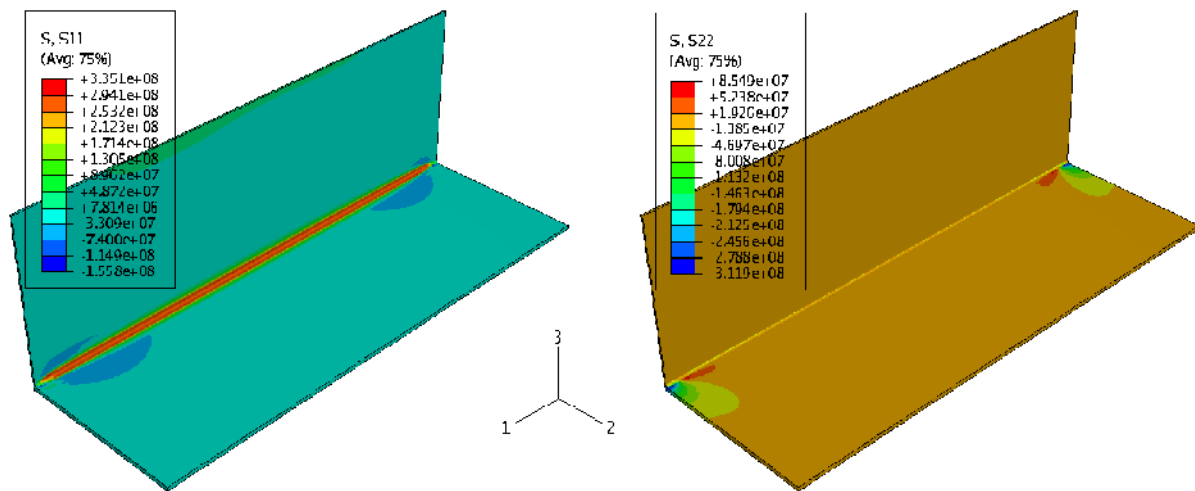


Fig. 10. Longitudinal (left) and Transverse (right) Residual Stress Distribution

2. Displacements measured by LVDT sensors and image correlation technique are in good agreement with numerical simulation results. Nevertheless, the difference in results may be explained on the basis of the assumptions like no gap between the base plate and stiffener, same material of the filler wire as that of T-joint etc.

3. Longitudinal residual stresses, σ_{xx} , have the values approaching yield strength of the material. Compared to all other stress components, they will have significant influence over the distortion pattern and the failure of the material. Moreover, the region of compressive stresses in HAZ may give rise to bending / buckling distortion.

4. Three dimensional elements with linear interpolation between the nodes are used both for thermal and mechanical analyses. Improvement in results may also be expected with quadratic interpolation between the nodes for mechanical analysis.

Any further improvement in FE simulation results may be expected by modelling the initial gap amongst the stiffener and the base plate, using the actual material properties for filler wire and taking care of the geometric imperfections of the base plate and the stiffener prior to welding.

REFERENCES

- [1] Sudnik, W., Radaj, D., Breitschwerdt, and S., Eroew, W., 2000, "Numerical Simulation of Weld Pool Geometry in Laser Beam Welding," J. Phys. D: Appl. Phys., 33, pp. 662–671.
- [2] Jin, X., Li, L., and Zhang, Y., 2003, "A Heat Transfer Model for Deep Penetration Laser Welding," Int. J. Heat Mass Transfer, 46, pp. 15–22.
- [3] Olmedo, M., 2004, "Soudage Laser en Aluminium," Masters thesis, ENISE France.
- [4] Tsirkas, S.A., Papanikos, P., and Kermanidis, Th., 2003, "Numerical Simulation of the Laser Welding Process in Butt-joint Specimens," J. Mater. Proc. Technol., 134, pp. 59–69.
- [5] Darcourt, C., Roelandt, J.-M., Rachik, M., Deloison, D., and Journet, B., 2004, "Thermomechanical Analysis Applied to the Laser Beam Welding Simulation of Aeronautical Structures," J. Phys. IV, 120, pp. 785–792.
- [6] Josserand, E., Jullien, J.F., Nelias, D., and Deloison, D., 2007, "Numerical Simulation of Welding-induced Distortions Taking into Account Industrial Clamping Conditions," Math. Modell. Weld Phenom, 8, pp. 1105–1124.

[7] Zaeem, M. A., 2007, "Prediction of Welding Buckling Distortion in a Thin Wall Aluminum T-joint," *Computational Materials Science*, 38, pp. 588–594.

[8] Zain-ul-abdein, M., Jullien, J.F., Nelias, D., and Deloison, D., 2009, "Prediction of Laser Beam Welding-induced Distortions and Residual Stresses by Numerical Simulation for Aeronautic Application," *Journal of Materials Processing Technology*, 209, pp. 2907–2917.

[9] Goldak, J., Chakravarti, A., and Bibby, M., 1984, "A new finite element model for welding heat sources," *Metall. Trans*, 15B, pp. 299–305.